Acousto-optic tomography with multiply scattered light

M. Kempe, M. Larionov, D. Zaslavsky, and A. Z. Genack

New York State Center for Advanced Technology on Ultrafast Photonics Materials and Applications, Department of Physics, Queens College of the City University of New York, Flushing, New York 11367

Received June 26, 1996; revised manuscript received September 19, 1996; accepted October 9, 1996

We have investigated the modulation of the optical field transmitted through a colloid of polystyrene spheres by a narrow quasi-cw ultrasound beam. Measurements of the scale dependence of the heterodyne modulation signal at the acoustic frequency are obtained for samples that are up to 140 scattering lengths thick. A calculation of the modulation signal predicts the possibility of tomographic imaging, which is confirmed experimentally. © 1997 Optical Society of America [S0740-3232(97)01305-7]

1. INTRODUCTION

Ballistic light can be used to image structures buried within a random medium with diffraction-limited resolution.[1,2] However, because its intensity decreases with sample thickness L as $\exp[-L(1/l_s + 1/l_a)]$, where l_s and l_a are the scattering length and the absorption length, respectively, the intensity of ballistic light typically falls below the shot-noise limit for $L/l_s \leqslant 30$. Since diffuse light decreases much more slowly with increasing opacity,[3] there has been intense interest in using diffuse light to image strongly scattering structures. The challenge of achieving high-resolution imaging with diffuse light has stimulated a variety of approaches.[4] These include the use of photon density waves arising from amplitude-modulated optical excitation[5] and the numerical reconstruction of time-resolved transmission measurements.[6] Another approach to imaging inhomogeneous media is to monitor the modulation of the transmitted light by an ultrasound beam traversing the sample. It is assumed that scattering of the acoustic beam is negligible. Marks *et al.* observed the variation in time of the transmitted optical intensity induced by an ultrasound pulse that is tightly focused within the sample.[7] The optical axis was perpendicular to the ultrasound axis, and the transmitted light was detected with use of a PIN photodiode. The photodiode signal was passed through a bandpass filter and the average of many digitized traces was taken. A signal is observed only from the focal region of the ultrasound. More recently, imaging through strongly scattering samples was accomplished with use of cw ultrasound[8] in a setup that is similar to the one in the pulsed acousto-optic (AO) experiments.[7] Imaging of structures under conditions expected in optical mammography remains a formidable challenge. In this paper we consider the origins of AO modulation and present a theoretical model of modulation by an acoustic beam that suggests that AO tomography is possible. We characterize the modulation of the field transmitted through a colloidal sample by a narrow ultrasound beam by measuring its dependence on parameters of the sample, sound and light. We then demonstrate AO tomography in a model system and assess the feasibility of this approach to mammography.

2. THEORETICAL CONSIDERATIONS

The passage of an acoustic beam of frequency ω_s through a scattering medium illuminated by a monochromatic laser at frequency ω creates a displacement $\mathbf{A}(\mathbf{r})\sin(\mathbf{k}_s \cdot \mathbf{r} - \omega_s t)$ within the medium, where $\mathbf{A}(\mathbf{r})$ is the amplitude of the displacement and $\mathbf{k}_s$ is the sound wave vector. This modulates a transmitted optical field at the period of the acoustic wave. We expect that the degree of modulation in the transmitted optical speckle pattern will be relatively suppressed when the acoustic beam overlaps absorbing structures in a body. In such structures the optical intensity is reduced and the impact of the acousto-optic interaction from such regions of the sample on the overall modulation is diminished. To consider the prospects for localizing absorbing structures within random media with use of measurements of the degree of optical modulation, we present a calculation of the dependence of this factor on the overlap of the optical and acoustic energies inside the medium. We are interested here in the interaction of a narrow acoustic beam with an optical field inside an inhomogeneous medium. A calculation and experimental demonstration of the modulation of multiply scattered light in the case in which a homogeneously disordered sample is excited by a uniform ultrasound field was carried out previously by Leutz and Maret.[9]

The field transmission coefficient for a partial wave that follows a path α through the sample from a source at $\mathbf{r}'$ at time t' to a detector at $\mathbf{r}$ at time t can be written as $p(\mathbf{r}, \mathbf{r}', t, t'; \alpha) = |p(\mathbf{r}, \mathbf{r}', t, t'; \alpha)| \exp[i\phi(t; \alpha) + i\psi(\alpha) - i\omega t]$, where the path α corresponds to a sequence of scattering events at n sites within the medium: $\phi = \mathbf{k}_0 \cdot (\mathbf{r}_1 - \mathbf{r}') + \mathbf{k}_1 \cdot (\mathbf{r}_2 - \mathbf{r}_1) + \cdots + \mathbf{k}_i \cdot (\mathbf{r}_{i+1} - \mathbf{r}_i) + \cdots + \mathbf{k}_n \cdot (\mathbf{r} - \mathbf{r}_n)$ is the part of the accumulated phase that is associated with the path length, where $\mathbf{k}_i$ is the wave vector of the partial wave after the ith scattering event and ψ is any additional phase shift associated with the scattering sequence. When the scat-

0740-3232/97/0501151-08$10.00

tering is isotropic, the scattering sites are separated by an average distance of the transport mean free path l and the average path length in the medium is $s = nl$. On the other hand, in the case of anisotropic scattering, temporal fluctuations in a homogeneously disordered system can be described in terms of the effective number of steps in the medium s/l.[10–13] The scattering sites move as a result of both the periodic displacement of the medium by the acoustic field and the random motion or flow within the sample. We assume here for concreteness that the fluctuations in position of successive scattering sites are not correlated. This is the case when the average separation of scattering sites is comparable to or greater than the acoustic wavelength. The modulation of the field can occur as a result of variations in the overall phase of the field transmission coefficient or of its magnitude. We expect that the phase variation is the dominant effect. The variation of the phase, $\Delta\phi(t + \tau, t) = \phi(t + \tau) - \phi(t)$, may result from a variation in the position of the scattering sites or of the magnitude of the scattering wave vector. The variation of the wave vector is due primarily to the modulation of the index of refraction of the medium by the acoustic wave. The modulation of the scatterer position and the optical wave vector can be treated on the same footing, and additional measurements are needed to determine their relative importance. The presence of the acoustic beam may also lead to a variation in the magnitude of the amplitude of the paths, $|p(\mathbf{r}, \mathbf{r}', t, t'; \alpha)|$, associated with scattering by the modulation of the index of refraction induced by the sound wave. If such modulation were to maintain a well-defined phase relationship to the acoustic field it might result in a coherent modulation of the total transmission.

To foster our examination of AO imaging, we focus on the optical modulation resulting from the displacement of scattering sites. The influence of the variation in the wave vector could readily be treated with use of the formalism presented here. The change in phase along path α between the observation times t and $t + \tau$ associated with the displacement of n scatterers along the path α as a function of time is given by

$$\Delta\phi(\mathbf{r}, \mathbf{r}'; t + \tau, t; \alpha) = -\sum_{j=1}^{n(\alpha)} \mathbf{q}_j \cdot \Delta\mathbf{r}_j(t + \tau, t), \quad (1)$$

where

$$\Delta\mathbf{r}_j(t + \tau, t) = \mathbf{A}(\mathbf{r}_j)\{\sin[\mathbf{k}_s \cdot \mathbf{r}_j - \omega_s(t + \tau)] - \sin(\mathbf{k}_s \cdot \mathbf{r}_j - \omega_s t)\} + \Delta\mathbf{r}_j'(t + \tau, t). \quad (2)$$

Here $\Delta\mathbf{r}_j'$ is the fluctuation in the displacement of the jth scatterer related to its random motion and $\mathbf{q}_j = \mathbf{k}_{j+1} - \mathbf{k}_j$ is the scattering vector. Since the fluctuations in the phase of a partial wave and the probability of following the associated trajectory are uncorrelated, the contribution to the field correlation function with time associated with a particular path α can be written as

$$G_1(\mathbf{r}, \mathbf{r}', \tau; \alpha) = \langle E(\mathbf{r}, \mathbf{r}', t + \tau; \alpha)E^*(\mathbf{r}, \mathbf{r}', t; \alpha)\rangle = I_0 P(\mathbf{r}, \mathbf{r}'; \alpha)\langle\exp[-i\Delta\phi(\mathbf{r}, \mathbf{r}', \tau; \alpha)]\rangle, \quad (3)$$

where I_0 is the specific intensity of the wave emerging from the source with wave vector $\mathbf{k}_0$, $P(\mathbf{r}, r'; \alpha) = \langle|p(\mathbf{r}, \mathbf{r}, t; \alpha)|^2\rangle$ is the probability that a photon will arrive at $\mathbf{r}$ from $\mathbf{r}'$ following the path α, and the angle brackets indicate the average over time t. The phase factor in the correlation function may be expressed as

$$\exp[-i\Delta\phi(\mathbf{r}, \mathbf{r}', \tau; \alpha)]\rangle = \exp\left[\sum_{j=1}^{n(\alpha)} i\mathbf{q}_j \cdot (\mathbf{A}(\mathbf{r}_j) \times \{\sin[\mathbf{k}_s \cdot \mathbf{r}_j - \omega_s(t + \tau)] - \sin(\mathbf{k}_s \cdot \mathbf{r}_j - \omega_s t)\} + \Delta\mathbf{r}_j')\right]. \quad (4)$$

Since the periodic and random displacements of different scatterers are uncorrelated, the time average of this factor can be written, once we expand the exponent, as

$$\langle\exp[-i\Delta\phi(\mathbf{r}, \mathbf{r}, \tau; \alpha)]\rangle = \left\langle \sum_{m=0}^{\infty} \frac{1}{m!}\left(\sum_{j=1}^{n(\alpha)} j\mathbf{q}_j \cdot \mathbf{A}(\mathbf{r}_j)\{\sin[\mathbf{k}_s \cdot \mathbf{r}_j - \omega_s(t + \tau)] - \sin(\mathbf{k}_s \cdot \mathbf{r}_j - \omega_s t)\}\right)^m \right\rangle \times \prod_{j=1}^{n(\alpha)} \langle\exp(i\mathbf{q}_j \cdot \Delta\mathbf{r}_j')\rangle. \quad (5)$$

Further, since there is no coherence between different partial waves arriving at a point, the only contributions to the field correlation function involve products of partial waves for the same path. Hence, the field correlation function is given by

$$G_1(\mathbf{r}, \mathbf{r}', \tau) = \sum_{\alpha} G_1(\mathbf{r}, \mathbf{r}', \tau; \alpha) \quad (6)$$

or

$$G_1(\mathbf{r}, \mathbf{r}', \tau) = I_0 \sum_{\alpha} P(\mathbf{r}, \mathbf{r}'; \alpha)\left\langle \sum_{m=0}^{\infty} \frac{1}{m!}\left(\sum_{j=1}^{n(\alpha)} i\mathbf{q}_j \cdot \mathbf{A}(\mathbf{r}_j)\{\sin[\mathbf{k}_s \cdot \mathbf{r}_j - \omega_s(t - \tau)] - \sin(\mathbf{k}_s \cdot \mathbf{r}_j - \omega_s t)\}\right)^m \right\rangle \times \prod_{j=1}^{n(\alpha)} \langle\exp(i\mathbf{q}_j \cdot \Delta\mathbf{r}_j')\rangle. \quad (7)$$

After averaging over all paths in the calculation of the correlation function, which corresponds to an average of the scattering vector over direction at each site, the linear term in $\mathbf{A}$ vanishes. We will consider the quadratic term, which is the leading term in this expansion for small dis-

placements. Since the scattering wave vectors at different sites for different paths are uncorrelated, we have in the quadratic term

$$\langle \mathbf{q}_j \cdot \mathbf{A}(\mathbf{r}_j)\mathbf{q}_{j'} \cdot \mathbf{A}(\mathbf{r}_{j'})\rangle = \langle [\mathbf{q}_j \cdot \mathbf{A}(\mathbf{r}_j)]^2\rangle \delta_{jj'}. \quad (8)$$

If we take the y direction to be along $\mathbf{A}$, this term is $\langle q_y{}^2 A^2\rangle$. But since the random medium is isotropic, $\langle q_y{}^2\rangle = \langle q^2/3\rangle$. For isotropic scattering $\langle q^2\rangle = 2k^2$, where k is the optical wave vector. The factor in Eq. (7) involving random displacements leads to an overall decay of the correlation function, which would be observed in the absence of the acoustic field, and will be denoted $\langle\langle \exp[i\Delta\phi'(\tau)]\rangle\rangle$.[10–13] Thus the correlation function related to the quadratic term in A is

$$G_1(\mathbf{r}, \mathbf{r}', \tau) = \frac{-k^2}{3} I_0 \sum_{\alpha} \sum_{j=1}^{n(\alpha)} P(\mathbf{r}, \mathbf{r}'; \alpha) A^2(\mathbf{r}_j) \times (1 - \cos \omega_s \tau) \langle\langle \exp[i\Delta\phi'(\tau)]\rangle\rangle. \quad (9)$$

To examine the consequences of the overlap of the optical and acoustic waves inside the sample, we express the probability density for following a particular path in terms of the coordinates within the sample. This can be done by noting that the probability of arriving at $\mathbf{r}$ from $\mathbf{r}'$ can be written as the product of the probability of reaching any particular scattering site $\mathbf{r}''$ from $\mathbf{r}'$ and the probability of reaching $\mathbf{r}$ from $\mathbf{r}''$:

$$P(\mathbf{r}, \mathbf{r}'; \alpha) = P(\mathbf{r}_j, \mathbf{r}'; \alpha) P(\mathbf{r}, \mathbf{r}_j; \alpha). \quad (10)$$

In the weak scattering limit, $kl \gg 1$, we may reverse the order of the summation so that instead of summing over each scattering site in every path, we sum over all paths that pass through each site. Further, since succeeding steps in the random walk of the photon are not correlated, we may sum separately over all paths α' that lead to the site $\mathbf{r}_i$ and over all paths α'' that lead away from that site to yield the following expression:

$$G_1(\mathbf{r}, \mathbf{r}', \tau) = \frac{-k^2}{3} I_0 \sum_{j=1}^{n(\alpha')} \sum_{\alpha'} \sum_{\alpha''} P(\mathbf{r}_j, \mathbf{r}'; \alpha') \times P(\mathbf{r}, \mathbf{r}_j; \alpha'') A^2(\mathbf{r}_j)(1 - \cos \omega_s \tau) \times \langle\langle \exp[i\Delta\phi'(\tau)]\rangle\rangle. \quad (11)$$

Since $I_0 \Sigma_\alpha P(\mathbf{r}_j, \mathbf{r}'; \alpha')$ is proportional to the intensity at $\mathbf{r}$, owing to a source at $\mathbf{r}'$, we may convert the sum over scatterers to an integral by multiplying the volume integral by the density of scatterers $1/l^3$. We sum over all source terms to obtain the correlation function at $\mathbf{r}$. This gives

$$G_1(\mathbf{r}, \tau) \propto \frac{-k^2}{3l^3} \int d\mathbf{r}'' I(\mathbf{r}'') P(\mathbf{r}, \mathbf{r}'') A^2(\mathbf{r}'') \times (1 - \cos \omega_s \tau) \langle\langle \exp[i\Delta\phi'(\tau)]\rangle\rangle. \quad (12)$$

This term is proportional to the volume integral of the product of the optical intensity, the probability that the light will arrive at $\mathbf{r}$, and the acoustic intensity. In transmission this term gives roughly equal weight to all points along the acoustic beam in the absence of absorption.

A quantity related to the field correlation function can be measured by beating the transmitted signal with a local oscillator (LO) field derived from the laser. The field correlation function is modulated at the fundamental and the harmonics of the acoustic frequency. By measuring the modulated signal as a function of the position of the acoustic beam, a tomographic image of the medium is obtained. Terms proportional to the higher harmonics of the acoustic wave may be relatively enhanced by increasing the intensity of the acoustic beam. This can be done by increasing the intensity at constant cross section for the beam or by focusing the beam. The signal related to higher-order terms in the acousto-optic interaction facilitates imaging from the focal region of the sound wave. Imaging in this mode can be achieved by scanning the focal region of the sound beam throughout the volume of the medium. In contrast to such point-by-point imaging, tomographic imaging can be accomplished by using an acoustic beam that is not sharply focused. In this case the signal comes from the entire length of the beam. This can accelerate data collection because the interaction along the entire length is sampled, reducing the time needed for signal averaging.

3. ACOUSTIC MODULATION SIGNAL

The experimental setup is shown in Fig. 1. The latex colloid sample and the ultrasound transducer are placed in a water tank. The ultrasound beam with a 2-mm-diameter waist and a confocal range of 5 cm is produced by a 2.54-cm-diameter transducer (f = 12 cm, Panametrics V380-SU). The transducer is driven by a quasi-cw electrical signal at 3.5 MHz, which consists of 50-μs-long pulses. The single-frequency argon–ion laser beam (λ = 514.5 nm) is collimated to a diameter of 6 mm. A beam splitter divides the beam into a part that illuminates the sample and a part that strikes the detector and serves as the LO for heterodyne detection. The light emerging from the sample is imaged onto a Si–PIN photodiode (New Focus 1801) by a 5-cm lens. The ac component of the photodiode signal is amplified and recorded by a digital storage oscilloscope synchronized to the excitation of the transducer and triggered 15 μs after the leading edge of the acoustic pulse. The data traces of 20-μs duration are

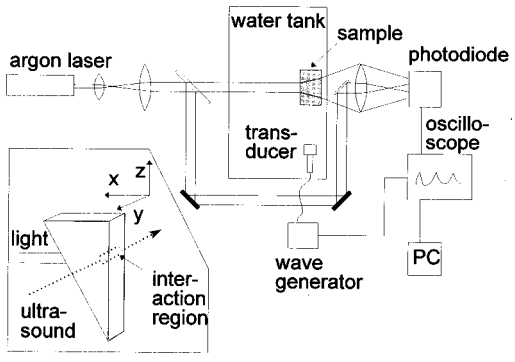

Fig. 1. Experimental setup. The inset shows the sample used.

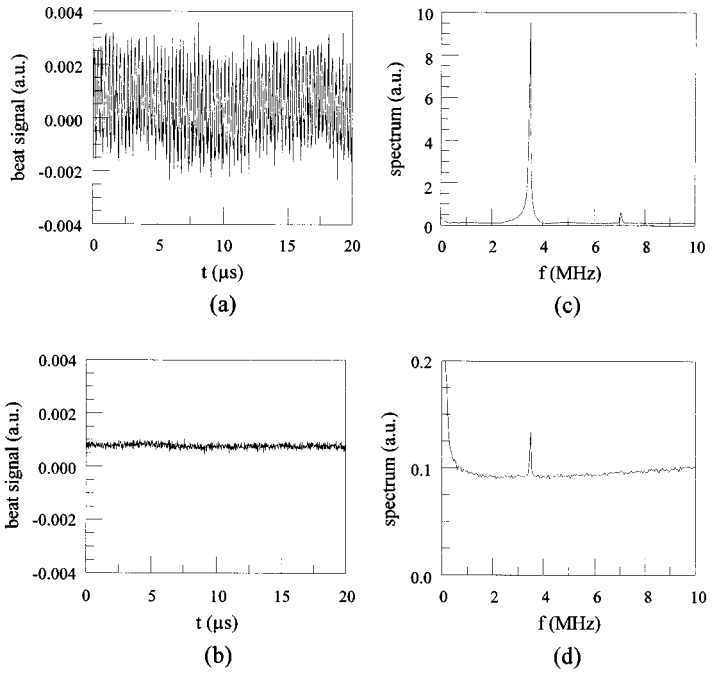

Fig. 2. (a), (b) Averaged data trace and (c), (d) averaged power spectra. The averages were performed over 50 traces for (a), (b) L/l_s = 10 and (c), (d) more than 2000 traces for L/l_s = 85.

transferred to a computer and Fourier transformed. The signal is the magnitude of the Fourier component of the heterodyne signal at 3.5 MHz subtracted from the noise background of the spectrum averaged over many data sets. This signal is related directly to the transmitted field rather than to the transmitted intensity. The colloid fills a wedge with glass windows so that the thickness of the sample can be varied by scanning the sample. The sides of the wedge are made of thin polyethylene sheet to minimize reflection of the sound beam. Latex spheres with 0.480-μm diameter in a solution with solid fraction between 0.00025 and 0.0068 are used. This gives scattering lengths l_s between 0.19 and 1.27 mm at 514 nm and an anisotropy factor of $g = 0.85$, according to Mie theory. The transport mean free path $l = l_s/(1 - g)$ is between 1.27 and 8.47 mm.

The average of the photodiode signal in the time domain and the average power spectrum for $L/l_s = 10$ and $L/l_s = 85$ are shown in Fig. 2. In the less opaque sample the heterodyne signal is predominantly due to ballistic light interacting at the Bragg angle with the ultrasound beam (0.2° from the perpendicular direction). The Bragg-scattered ballistic light experiences a frequency shift and is deflected at twice the Bragg angle from the original direction of propagation. We find that the intensity detected in the heterodyne signal falls exponentially with a slope $1/l_s$, the value of l_s being the one calculated from Mie theory (see Fig. 3). For $L/l_s \geq 20$, however, the signal falls considerably more slowly. This signal is due to multiply scattered light.

Note that the signal in the multiply scattering regime is larger for smaller l_s at the same ratio L/l_s. Though for a given L/l_s the total transmission through the sample is the same, the fraction of light that falls on the detector is proportional to A_d/A, where A_d is the area of the detector and A is the area of the diffuse light on the back side of the sample. In the absence of absorption we expect $A \propto L^2$. To factor out the dependence of the signal on the area of the sample illuminated by diffuse light, we multiply the signal from Fig. 3 by the sample thickness. The results are shown in Fig. 4. The fit to the modified signal yields a power dependence $(L/l)^p$ with $p = 1.1 \pm 0.1$, which is twice as large as expected for a signal that scales like the square root of the total transmission through a slab. This faster falloff could be due to the

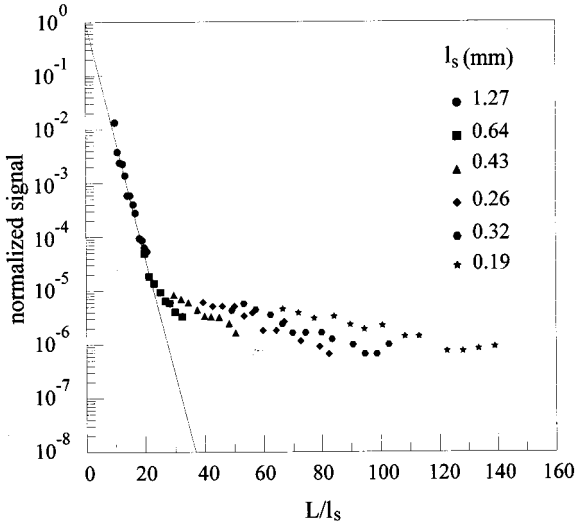

Fig. 3. Heterodyne signal normalized to the signal in clear water for various concentrations of latex spheres in water. For each concentration the sample thickness was varied from 12 to 30 mm. The signal falloff for ballistic light according to Mie theory is shown as solid line. The LO beam was wave front matched to the ballistic light, and the Bragg condition was satisfied.

leakage of light out the sides of the sample, which has the shape of a triangular prism. The signal is also reduced by the presence of absorption. If we assume that the absorption length in water is $l_a = 3$ m, the absorption attenuation length[3] $L_a = \sqrt{l l_s/3}$ for the sample with a mean free path of 1.29 mm is 36 mm. This is comparable to the size of the thickest samples studied.

We investigated the dependence of the signal on the shape of the wave front of the LO field and on the angle between the optic and the acoustic axes. The difference between the signal on and off the optic axis disappeared when either the wave-front matching condition or the Bragg condition for ballistic light was not satisfied. In contrast, the signal for $L/l_s \geqslant 20$ is found to be independent of these factors, as would be expected if the transmitted field were incoherently related to the LO field.

The coherence time of the transmitted light in our sample is longer than the length of a data trace (20 μs).

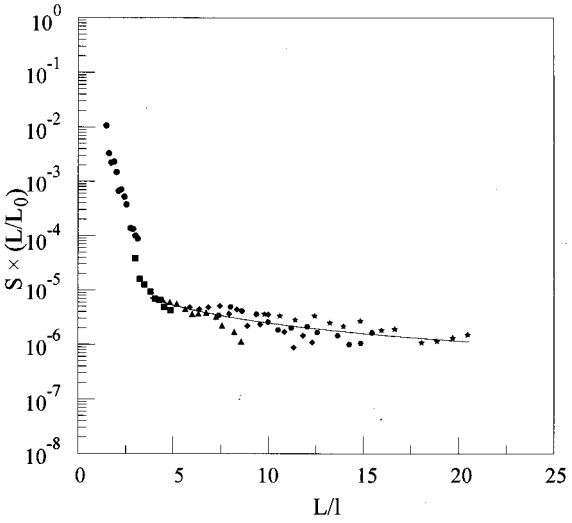

Fig. 4. Same signal as in Fig. 3 normalized by L_0/L with $L_0 = 16$ mm as a function of L/l. The solid curve is a fit to the data according to a power law L^p.

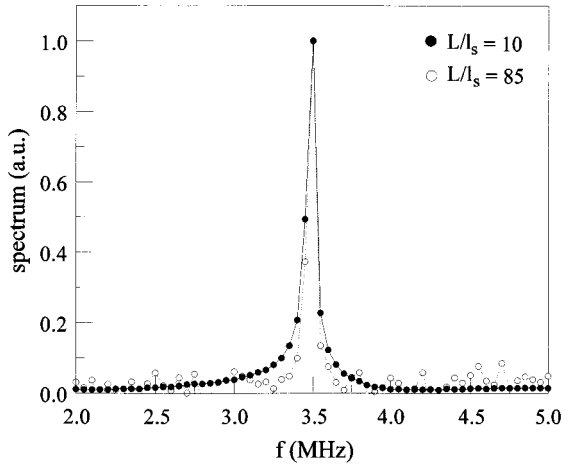

Fig. 5. Normalized spectra from Fig. 2 in the neighborhood of $f = 3.5$ MHz.

This is evident from the spectral width of the peak at 3.5 MHz, which is limited by the finite record length in the ballistic as well as the diffusive regime (see Fig. 5). Successive data traces are recorded at times separated by a few hundred milliseconds, which is longer than the coherence time for the heterodyne signal. Since averaging over n spectra reduces the noise by $n^{1/2}$, the signal-to-noise S/N ratio improves by this factor. In contrast, averaging of the data traces reduces both the signal and the noise, and the SNR is not improved.

In the diffuse regime, the signal drops by a factor of approximately 7 to 10 if the argon–ion laser is used in multimode as opposed to single-mode operation. If the approximately 50 modes of the multimode laser have a mode spacing larger than the width of the field correlation function,[3] each mode produces an independent speckle pattern.[14] The total degree of modulation should then be reduced by the square root of the number of modes, as is observed. This indicates that the intensity in the speckle patterns is not coherent with the acoustic modulation. This is consistent with the absence of an observable modulation signal when the sample is illuminated with white light derived from a flashlight.[15]

To obtain an expression for the heterodyne signal resulting from the modulation of the speckle pattern, we start with a consideration of the intensity at a given point on the detector. It is

$$\begin{aligned} I &= |E_{\mathrm{LO}} + E_T|^2 \\ &= |E_{\mathrm{LO}}|^2 + |E_T|^2 + 2|E_{\mathrm{LO}}|m|E_T|\cos(\omega_s t + \varphi) \\ &\quad + 2|E_{\mathrm{LO}}|(1 - m)|E_T|\cos(\psi), \end{aligned} \tag{13}$$

where E_{LO} and E_T are the LO field and the transmitted field, respectively. The local degree of modulation is $m = |E_T(\omega \pm \omega_s)|/|E_T|$, where $E_T(\omega \pm \omega_s)$ is the part of the transmitted field that is shifted by a frequency ω_s as a result of phase or amplitude modulation by the sound. The phase of the unmodulated part of the transmitted field relative to the phase of the LO field is denoted by ψ, and the relative phase of the modulated part of the transmitted field is denoted by φ. The total signal measured by the detector is obtained by integrating over the detector area to give the product of the detector area, A_d, and the average of the local intensity, $\langle I \rangle$. This yields

$$\begin{aligned} A_d\langle I\rangle = A_d[&\langle|E_{\mathrm{LO}}|^2\rangle + \langle|E_T|^2\rangle \\ &+ \langle 2|E_{\mathrm{LO}}|m|E_T|\cos(\omega_s t + \varphi)\rangle \\ &+ \langle 2|E_{\mathrm{LO}}|(1 - m)|E_T|\cos(\psi)\rangle]. \end{aligned} \tag{14}$$

If we assume that the LO field is uniform over the detector and that the modulation phase in different coherence areas is uncorrelated, the heterodyne term is

$$2A_d|E_{\mathrm{LO}}|\langle m\rangle\langle|E_T|\rangle\langle\cos(\omega_s t + \varphi)\rangle.$$

In addition there is a contribution to the heterodyne signal resulting from the transmitted light alone: $2A_d\langle(1 - m)m\rangle\langle|E_T|^2\rangle\langle\cos(\omega_s t + \varphi - \psi)\rangle$. In our case this contribution is negligible compared with the term involving the LO. If the transmitted field has a variance as large as its average value, which is approximately true for diffuse light,[14] we have $\langle|E_T|\rangle = (\langle|E_T|^2\rangle/2)^{1/2}$. Further-

more, $\langle \cos(\omega_s t + \varphi) \rangle = \cos(\omega_s t + \varphi')/N^{1/2}$, where N is the number of coherence areas. Thus the signal at the frequency of the ultrasound would be

$$S \propto (2P_{\mathrm{LO}} P_T)^{1/2} m_{\mathrm{eff}}, \tag{15}$$

with an effective degree of modulation $m_{\mathrm{eff}} = \langle m \rangle / N^{1/2}$, where $P_{\mathrm{LO}/T} \propto A_d \langle |E_{\mathrm{LO}/T}|^2 \rangle$ is the power detected that is associated with the LO and the transmitted light, respectively.

In the absence of absorption, the illuminated area on the back of the sample is approximately L^2. Because this is considerably larger than the detector area $A_d \approx 0.6$ mm^2, the size of the coherence area in the detector plane is given by $A_c \approx \lambda^2 s^2 / A_l$, where s is the lens–detector distance and A_l is the area of the aperture of the imaging lens.[14] With our experimental values, $s = 70$ mm and $A_l \approx 700$ mm^2, we obtain $A_c \approx 2 \times 10^{-6}$ mm^2. Thus the number of coherence areas on the detector is $A_d / A_c \approx 3 \times 10^5$. We would expect, therefore, that the effective degree of modulation is given by $m_{\mathrm{eff}} = \langle m \rangle / N^{1/2} \approx 2 \times 10^{-3} \langle m \rangle$. The observed degree of modulation is of order 2×10^{-4} at $L/l_s = 85$. This would suggest a degree of modulation of a single coherence area of the order of 10%. To check whether the contributions of each coherence area to the signal are uncorrelated, as was assumed in our estimate, we evaluate the actual dependence of m_{eff} on the number of coherence areas on the detector by measuring its dependence on the diameter of the aperture of the imaging lens, d. Because A_c is inversely proportional to $A_l \propto d^2$, one has $N \propto d^2$. If the effective degree of modulation was reduced by the square root of the number of coherence areas on the detector, as discussed above, it would be inversely proportional to the aperture diameter. In the experiment, we observe $m_{\mathrm{eff}} \propto d^{-p}$ with $p = 0.70 \pm 0.04$ for our sample with $L/l_s = 85$. Thus we find $m_{\mathrm{eff}} \approx \langle m \rangle / N^{0.35}$ for the range of N from $\approx 1.5 \times 10^3$ to $\approx 3 \times 10^5$. Extrapolating this function to $N = 1$ leads to the conclusion that the degree of modulation in a single coherence area is 2%. This seems to indicate the presence of long-range correlation in the signal contributed by each coherence area. This situation might arise if the phase of the modulation varied on a larger scale than that of the transmitted field itself. This question will be explored in future work in which the degree of modulation for both smaller and larger values of N than studied here will be measured.

A vital issue that needs to be addressed is the fundamental limits of the technique resulting from the achievable S/N ratio. In the heterodyne as well as in the homodyne techniques,[7,8] the ultimate S/N ratio is shot-noise limited. For the thickest sample investigated ($L/l_s \approx 140$), we have a power of $\approx 5 \times 10^{-13}$ W in the modulated transmitted light. This is approximately what one expects from the transmitted light falling on the photodiode and the observed effective degree of modulation. With a detector integration time of $t = 100$ ms, we are therefore approximately 360 times above shot noise. Assuming no correlations among the coherence areas, the shot-noise limit in the signal when many coherence areas fill the detector area is the same as that in a single coherence area, $S/N_s = [P_0 T t / (N E_p)(\Omega_s / 2\pi)]^{1/2} \langle m \rangle$, where E_p is the photon energy, $N \approx \pi^2 L_a L / (4\lambda^2)$ is the number of coherence areas on the sample's surface, Ω_s is the solid angle of detection, and $T \approx (l/l_a)^{1/2} \exp[-L/L_a]$ is the total transmission through the sample. In the case of weak absorption ($L < L_a$), we have $N \approx \pi^2 L^2 / (4\lambda^2)$ and $T \approx l/L$. For our thickest sample, this gives $N \approx 10^{10}$, $\Omega_s / 2\pi = 3 \times 10^{-3}$; and with $P_0 = 100$ mW and $t = 100$ ms we obtain $S/N_s \approx 20 \langle m \rangle \approx 2$. The fact that the SNR observed by averaging over $< 10^5$ coherence areas is larger than this value is in accord with the observed deviation of the scaling of m_{eff} from the expected $1/\sqrt{N}$ behavior.

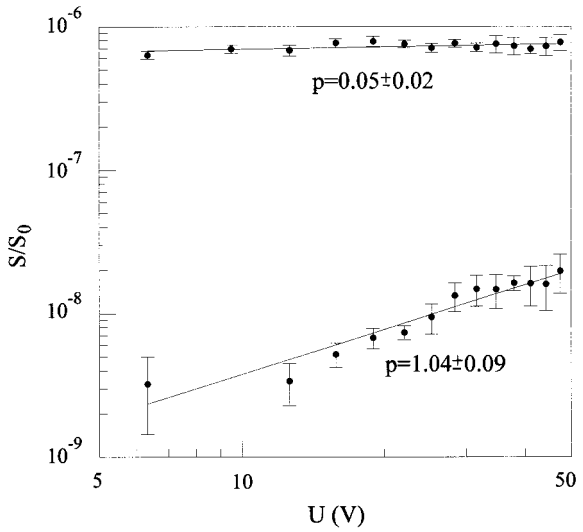

Fig. 6. Signal for $L/l_s = 20$ (upper curve) and $L/l_s = 45$ (lower curve) normalized to the signal in clear water as a function of driving voltage of the transducer. The water signal is linear in U (slope: 1.01 ± 0.01) in the voltage range considered. In the diffusive regime, however, the dependence changes from linear to quadratic.

4. IMAGING OF ABSORBING STRUCTURES

Based on the calculations presented in Section 2, a tomographic mapping of the differential absorption in a sample is possible with the AO technique, with use of diffuse photons. In this section we provide a proof-of-principle demonstration of this capability.

One prediction of the calculations is that the signal in the diffusive regime is proportional to the intensity of the ultrasound as opposed to the situation in the ballistic regime, where the signal is proportional to the amplitude of the sound. The measurements of the signal as a function of the transducer driving voltage (Fig. 6) in the ballistic and the diffusive regimes confirm this prediction. The same result has been found by Leutz and Maret, where the whole sample was excited by a plane sound wave.[9]

Another issue concerns the variation of the signal as a function of scan position of the ultrasound beam. Equation (12) shows that the signal depends on the product of the light intensity at a given point in the sample and the probability that a photon reaches the detector from this point. Thus one expects only a weak dependence of the signal on the sound position as the beam is scanned along

the axis connecting the point of incidence and detection. The experimental result is shown in Fig. 7. Interestingly, the signal near the back side of the sample is even higher than the signal near the point of incidence of the light. This may be a result of the closeness of the detector to the ultrasound beam in this case. A significant variation of the signal on the position of the ultrasound beam would result in a change of contrast of objects imaged at different distances from the source–detector axis and would complicate imaging in large samples. (In this case, one might need to reposition the detector and the point of incidence to obtain sufficient signal from the edges of a sample.)

The following experiment in an inhomogeneous sample was carried out to demonstrate the concept of tomographic imaging. We use a black Teflon sphere of 5-mm diameter as the object and scan the transducer across the sample (x direction in Fig. 1) in which the sphere is immersed. The sphere partially reflects and partially absorbs the ultrasound. For various positions of the sphere in the y direction we obtain a signal as shown in Fig. 8(a). The contrast in the image is due to absorption of the light and the sound in the sphere. From an image taken in clear water, we determine the resolution that one would observe with ballistic light (approximately given by the diameter of the sound beam of 2 mm) and the sound absorption. A consideration based on Eq. (12) allows us to predict the image in the scattering medium [see Fig. 8(b)]. We make the simplifying assumption that the product $P(\mathbf{r}, \mathbf{r}')I(\mathbf{r}')$ from Eq. (12) is a constant throughout the sample and A^2 is constant within a pencil of 2-mm diameter. In the sphere nearly all the incident light is absorbed while the surrounding medium is nearly absorption free. Then the maximum contrast in the signal for a given position of the sphere is $(S_{\max} - S_{\min})/(S_{\max} + S_{\min})$ with $S_{\max} = V_1 + V_2 + V_{\text{sph}}$ and $S_{\min} = V_1 + V_2 T_{\text{sound}}$, where V_1 and V_2 are the volume occupied by the pencil in the sample before hitting the sphere and after transmission through the sphere, respectively, V_{sph} is the volume of the sphere intercepted by the sound beam, and T_{sound} is the transmission coefficient of the sound through the sphere. The predicted signal is in reasonable agreement with the observed signal (see Fig. 8). There is some loss of resolution, which can be attributed to the influence of the absorbing structure beyond its boundary as a result of the diffusion of photons. This effect might facilitate the detection of small, weakly absorbing structures by increasing the sensitivity of the technique.

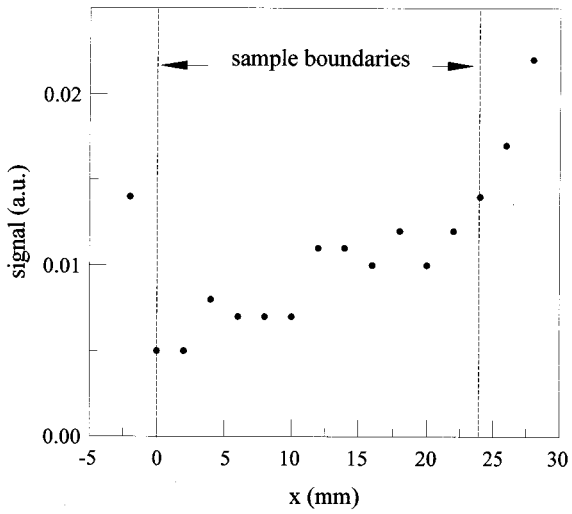

Fig. 7. Signal as a function of scan position in the sample. The light is incident on the left sample boundary.

5. DISCUSSION

One can estimate the image contrast in breast tumor diagnosis from the above considerations. A large range of optical parameters are reported for the breast. Approximate sample parameters at 670 nm are[16] $l = 1$ mm and $l_a = 500$ mm. At 800 nm, an absorption length as short as 100 mm has been observed.[17] We use the following parameters: $l_a - 500$ mm in the normal breast tissue,

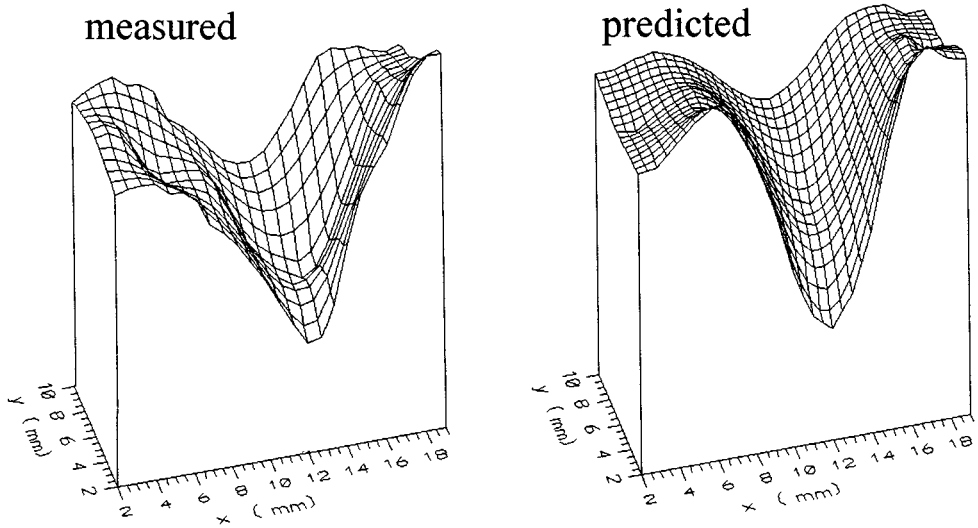

Fig. 8. On the left, scans of the sound across a black teflon sphere at various positions y within the sample ($L/l_s = 37$). On the right, predicted signal as explained in the text.

$l_a = 25$ in the tumor, a sample thickness of $L = 50, ..., 80$ mm, a tumor with diameter $d = 5$ mm in the middle of the sample, and a sound beam with a diameter of 2 mm. In the tumor, the light intensity is reduced compared with the normal tissue by a factor of about 1.5. On the other hand, the tumor has nearly the same properties with regard to the sound wave as the surrounding tissue. The maximum contrast under these conditions is then ≈ 0.02. To localize objects with such a contrast, a S/N ratio of at least 50 to 100 is required. If we consider an incident light intensity $P_0 = 100$ mW at $\lambda = 670$ nm and a detection integration time $t = 100$ ms, we obtain for the S/N ratio in a single coherence area $(S/N)_s \approx 20$ to 100 $\langle m \rangle$. Thus the required S/N ratio for breast tumor diagnosis with the present imaging modality cannot be obtained if it is limited by the shot noise in a single coherence area.

A number of approaches may be taken to enhance the S/N ratio for tomographic imaging. The intensity in a single coherence area can be increased by coating the breast with a strongly scattering suspension such as a titania colloid or with a scattering or a reflecting solid and extracting the light to be detected, using an optical fiber. Photons that leave the sample near the point of incidence would be reinjected into the breast, and the effective incident intensity would be enhanced. Further, the intensity near the collecting fiber would be enhanced over the value at the surface of the uncovered breast because photons are internally reflected at nearby regions of the surface. This can result in an enhancement by two orders of magnitude in the intensity detected and an order of magnitude in the S/N ratio.[18] Perhaps the most striking feature of AO imaging is the fact that the signal essentially resides in a single coherence area. Since N can be larger than 10^{10} it is a challenge to find ways to use multichannel detection to enhance the S/N ratio. Finally, the correlation in the signal from different coherence areas of the speckle pattern appears to give a S/N ratio for the signal from many coherence areas, which is larger than that expected for quantum-limited detection in a single coherence area. Further study of this effect is required to assess whether this can significantly enhance the S/N ratio of tomographic imaging.

In conclusion, our experiments show that AO tomographic imaging is possible. Definite conclusions concerning the applicability of the AO technique to optical mammography cannot be drawn until various means for enhancing the signal are explored. In any case, the tomographic approach could be useful for a variety of types of medical imaging in tissues that are optically less opaque than the breast.

ACKNOWLEDGMENTS

This work is supported by National Science Foundation Grant DMR 9632789 and by a PSF–City University of New York grant. We thank R. L. Weaver for discussions and for the use of the acoustic transducer. We also thank A. A. Lisyansky for discussions.

REFERENCES

1. J. A. Izatt, M. R. Hee, G. M. Owen, E. A. Swanson, and J. G. Fujimoto, "Optical coherence microscopy in scattering media," Opt. Lett. **19**, 590–592 (1994).
2. M. Kempe and W. Rudolph, "Scanning microscopy through thick layers based on linear correlation," Opt. Lett. **19**, 1919–1921 (1994).
3. A. Z. Genack, "Transmission in disordered media," Phys. Rev. Lett. **58**, 2043–2046 (1987).
4. R. R. Alfano, ed., *Advances in Optical Imaging and Photon Migration*, Vol. 21 of OSA Proceedings Series (Optical Society of America, Washington, D.C., 1994).
5. M. A. O'Leary, D. A. Boas, B. Chance, and A. G. Yodh, "Experimental images of heterogeneous turbid media by frequency domain diffusing-photon tomography," Opt. Lett. **20**, 426–428 (1995).
6. J. C. Hebden and D. T. Delpy, "Enhanced time-resolved imaging with a diffusion model of photon transport," Opt. Lett. **19**, 311–313 (1994).
7. P. A. Marks, H. W. Tomlinson, and G. W. Brooksby, "A comprehensive approach to breast cancer detection using light: photon localization by ultrasound modulation and tissue characterization by spectral discrimination," in *Photon Migration and Imaging in Random Media and Tissues*, R. R. Alfano and B. Chance, eds., Proc. SPIE **1888**, 500–510 (1993).
8. L. Wang, S. L. Jacques, and X. Zhao, "Continuous-wave ultrasonic modulation of scattered laser light to image objects in turbid media," Opt. Lett. **20**, 629–631 (1995).
9. W. Leutz and G. Maret, "Ultrasonic modulation of multiply scattered light," Physica B **204**, 14–19 (1995).
10. G. Maret and P. E. Wolf, "Multiple light scattering from disordered media. The effect of Brownian motion of scatterers," Z. Phys. B **65**, 409–413 (1987).
11. M. J. Stephen, "Temporal fluctuations in wave propagation in random media," Phys. Rev. B **37**, 1–5 (1988).
12. D. J. Pine, D. A. Weitz, P. M. Chaikin, and E. Herbolzheimer, "Diffusing-wave spectroscopy," Phys. Rev. Lett. **60**, 1134–1137 (1988).
13. A. G. Yodh, P. D. Kaplan, and D. J. Pine, "Pulsed diffusing-wave spectroscopy: High resolution through nonlinear optical grating," Phys. Rev. B **42**, 4744–4747 (1990).
14. J. W. Goodman, *Statistical Optics* (Wiley, New York, 1985).
15. L. Wang, X. Zhao, and S. L. Jacques, "Ultrasound modulated optical tomography," in *Advances in Optical Imaging and Photon Migration*, R. R. Alfano and J. G. Fujimoto, eds., Vol. 2 of 1996 TOPS (Optical Society of America, Washington, D.C., 1996).
16. B. Chance, K. Kang, and E. Sevick, "Photon diffusion in breast and brain: Spectroscopy and imaging," Opt. Photon. News **4**, 9–13 (1993).
17. J. C. Hebden, D. J. Hall, M. Firbank, and D. T. Delpy, "Time-resolved optical imaging of a solid tissue-equivalent phantom," Appl. Opt. **34**, 8038–8047 (1995).
18. N. Garcia, A. Z. Genack, and A. A. Lisyansky, "Measurement of the transport mean free path of diffusing photons," Phys. Rev. B **46**, 14475–14479 (1992).